ANKARA UNIVERSITY
INSTITUTE OF NUCLEAR SCIENCES

MASTER THESIS

MEASUREMENT OF URANIUM, THORIUM AND POTASSIUM ACTIVITY CONTENT IN BEYLİKOVA-SİVRİHİSAR COMPLEX ORE SITE AND ESTIMATION OF DOSE RATES TO MINERS

SÜLEYMAN ÖVÜÇ

DEPARTMENT OF MEDICAL PHYSICS

HEALTH PHYSICS MASTER'S PROGRAM

ANKARA

2019

THESIS APPROVAL

The thesis entitled "Measurement of uranium, thorium and potassium activity content in Beylikova-Sivrihisar complex ore site and estimation of dose rates to the miners" prepared by Süleyman ÖVÜÇ in partial fulfillment of the requirements for the degree of Master of Science in Health Physics Program of the Medical Physics Department of Institute of Nuclear Sciences in Ankara University and has been examined and approved by the undersigned jury members.

Supervisor: Prof. Dr. Haluk YÜCEL

Jury Members:

Prof. Dr. Mehmet TOMBAKOĞLU

Hacettepe University Nuclear Energy Engineering

Prof. Dr. Ali Ulvi YILMAZER

Ankara University Department of Physics Engineering

Prof. Dr. Haluk YÜCEL

Ankara University Institute of Nuclear Sciences

The result above is approved.

Prof. Dr. Niyazi MERİÇ

Head of the Institute

I hereby declare that all information in this thesis has been obtained and presented in accordance with academic rules and ethical conduct. I also declare that, as required by these rules and conduct, I have fully cited and referenced all material and results that are not original to this work.

Name, Last Name: Süleyman ÖVÜÇ

Signature: 

ABSTRACT

Master Thesis

MEASUREMENT OF URANIUM, THORIUM AND POTASSIUM ACTIVITY CONTENT IN BEYLİKOVA-SİVRİHİSAR COMPLEX ORE SITE AND ESTIMATION OF DOSE RATES TO MINERS.

Süleyman Övüç

Ankara University Institute of Nuclear Sciences

Department of Medical Physics

Health Physics Master Degree Program

Supervisor: Prof. Dr. Haluk YÜCEL

In this thesis, the activity concentrations of uranium (^{238}U), thorium (^{232}Th) and potassium (^{40}K) nuclides in the complex ore samples containing rare earth element (REE) oxides obtained from the region of Beylikova-Sivrihisar ore site of ETİMADEN Corporate were determined by a high resolution gamma-ray spectrometry with a n-type, 78.5% Ge detector. A total of 60 ore samples were taken from five different locations in ore site. One location is inside the gallery and the others are marked in the scaling map of the mine site. The mean activity values were calculated as 2135±35 Bq·kg^{-1} (min: 63±23 to max: 4793±54 Bq·kg^{-1}) for ^{238}U, 1749±3 Bq·kg^{-1} (min: 52±1 to max: 6030±10 Bq·kg^{-1}) for ^{226}Ra, 3773±5 Bq·kg^{-1} (min: 431±1 to max: 6704±13 Bq·kg^{-1}) for ^{232}Th and 324±2 Bq·kg^{-1} (min: 40±2 to max: 1149±4 Bq·kg^{-1}) for ^{40}K. From the measured activity results, the possible external and internal gamma doses and health hazard indexes were calculated for mine workers in case it was mining in an open mine gallery. For inside gallery, external health hazard index is estimated to be 33.5±0.02 and internal health hazard index is 45.9±0.02, which are always greater than unity given for public. While the maximum external gamma dose calculated to be 3.1 mSv·y^{-1} in the gallery, and 1.54 mSv·y^{-1} for open area, mean gamma dose values calculated to be 1.85 mSv·y^{-1} in the gallery and 0.93 mSv·y^{-1} for open area. These estimated annual doses for mine workers are due to mainly ^{226}Ra and ^{232}Th decay series nuclides. The results indicate that health hazard indexes can be reduced remarkably when open gallery mining is carried out by considering the necessary radiation protection measures, especially using radon gas reduction techniques.

July 2019, 51 pages

Key words: Gamma-ray spectrometry, HpGe detector, radioactivity, reference material, self-absorption, rare earth element, ore, dose, health hazard index

ÖZET

Yüksek Lisans Tezi

BEYLİKOVA-SİVRİHİSAR KOMPLEKS CEVHER SAHASINDA URANYUM, TORYUM VE POTASYUM AKTİVİTELERİNİN ÖLÇÜLMESİ VE MADENCİLERİN ALABİLECEĞİ DOZ ORANLARININ TAHMİNİ

Süleyman Övüç

Ankara Üniversitesi Nükleer Bilimler Enstitüsü

Medikal Fizik Anabilim Dalı

Sağlık Fiziği Yüksek Lisans Programı

Danışmanı: Prof. Dr. Haluk YÜCEL

Bu tez çalışmasında, Beylikova-Sivrihisar bölgesinde bulunan, Etimaden nadir toprak elementlerini bulunduran kompleks cevher sahasındaki numuneler üzerinde uranyum (^{238}U) toryum (^{232}Th) ve potasyum (^{40}K) nükleidlerinin aktivite konsantrasyonları n tipi, % 78,5 verim değerine sahip Ge detektörlü, yüksek çözünürlüklü bir gama ışını spektrometresi ile belirlenmiştir. Cevher sahasındaki beş farklı yerden toplam 60 cevher numunesi alınmıştır. Bu beş farklı noktadan biri galeri içerisinde yer almakta olup diğerleri ise maden sahasının ölçeklendirme haritasında gösterilmektedir. Ortalama aktivite değerleri ^{238}U için 2135±35 $Bq{\cdot}kg^{-1}$ (min: 63±23 max: 4793±54 $Bq{\cdot}kg^{-1}$), ^{226}Ra için 1749±3 $Bq{\cdot}kg^{-1}$ (min: 52±1, max: 6030±10 $Bq{\cdot}kg^{-1}$), ^{232}Th için 3773±5 $Bq{\cdot}kg^{-1}$ (min: 431±1, max: 6704±13 $Bq{\cdot}kg^{-1}$), ve ^{40}K için 324±2 $Bq{\cdot}kg^{-1}$ (min: 43±2, max: 1149±4 $Bq{\cdot}kg^{-1}$) olarak hesaplandı. Ölçülen aktivite sonuçlarından, maden işçileri için olası iç ve dış gama dozları ve sağlık tehlikesi indisleri hesaplandı. İç galeride, dış sağlık tehlikesi indisi 33,5±0.02, iç sağlık tehlikesi indisi 45,9±0.02 ve halk için birlikten daha az olmalıdır. Galeride 3,1 $mSv{\cdot}y^{-1}$ ve açık alanda 1,54 $mSv{\cdot}y^{-1}$, olarak hesaplanan maksimum gama dozu, galeride ortalama 1,85 $mSv{\cdot}y^{-1}$ ve açık alanda ortalama 0,93 $mSv{\cdot}y^{-1}$ olarak hesaplandı. Maden işçileri için tahmini dozlar esas olarak ^{226}Ra ve ^{232}Th serisi nüklidlerden kaynaklanmaktadır. Sonuçlar, gerekli radyasyondan korunma önlemleri dikkate alınarak, özellikle radon gazını azaltma teknikleri kullanılarak açık galeri madenciliği yapıldığında sağlık tehlikesi indislerinin önemli ölçüde azaltılabileceğini göstermektedir.

Temmuz 2019, 51 sayfa

Anahtar kelimeler: Gama spektrometre, HpGe dedektörü, radyoaktivite, referans malzeme, öz soğurma, nadir toprak elementi, cevher, doz, sağlık tehlikesi indisi

ACKNOWLEDGEMENTS

First of all, praise is only to almighty Allah.

I would like to thank my supervisor Prof. Dr. Haluk Yücel who shed light on me in my works and also thanks for his excellent advices. I am gratefully thankful to the Dr. Gizem Akkaya, who is in post-doctoral personnel in Institute of Nuclear Sciences for her valuable scientific suggestions and personal supporting during my all thesis's work.

I would like to thank Etimaden General Directorate for the cooperation they made during the discovery of mining area and for their help with the permission number 50894663-103.01 for taking samples procedure. In this context, I would like to thank Mehmet Candemir, a geological engineer from Etimaden who has been authorized to introduce the ore site to us.

Additionally, I would like to thank to the administrative personnel in Institute of Nuclear Sciences for their support, and I am also appreciated to İbrahim Demirel for help in the writing of this thesis.

Last but not the least I am heartily grateful to my wife and my family members who supported and encouraged me a lot during my studies, their good wishes always accompanied me.

TABLE OF CONTENTS

LIST OF SYMBOLS AND ABBREVIATIONS

A	Activity
Bq	Becquerel (disintegration per second)
Ci	Curie (1 Ci = $3.7x10^{10}$ Bq)
CVO	Coefficient-of-variation
D	Absorbed Dose
ED_{in}	Effective Dose Indoor
ED_{out}	Effective Dose Outdoor
EPA	Environmental Protection Agency
eV	Electronvolt
f_γ	Gamma emission probability
F_{coi}	True coincidence correction factor
FWHM	Full With Half Maximum
Gy	Gray
H_{in}	Internal Health Hazard Index
H_{ext}	External Health Hazard Index
HpGe	High Purity Germanium
I	Gamma Concentration Index
IAEA	International Atomic Energy Agency
ICRP	International Commission on radiological protection
keV	Kilo Electronvolt
MeV	Million Electronvolt
$t_{1/2}$	Half Life
WHO	World Health Organization
ε	Detection Efficiency
λ	Decay Constant
μ	Linear Attenuation coefficient (cm^{-1})
τ	Mean Life Time

FIGURE LIST

TABLE LIST

1. INTRODUCTION

Ionizing radiation is always in our daily life because of the terrestrial and cosmic radiations. Normally we are exposed by external and internal radiation sources in routine life where we live, and sometimes during the medical examinations or occupational activities. In this context, the sources can be divided two categories that artificial sources and natural sources. Exposure to natural background radiation is an integral part of human existence on earth. As shown in Figure 1 the natural radiation caused most important contribution to public exposure (average: 2.4 $mSv \cdot y^{-1}$) in the World according to average environmental radiation results that above the %71. (IAEA, 2019).

Human being is exposed to ionizing radiation from natural sources in two way, one of them is cosmic rays entering the earth's atmosphere from outer space and the second one is the radionuclides, ^{238}U and ^{232}Th and their decay series and ^{40}K, naturally occurring in earth crust such as soil and stones. These radionuclides caused two different type exposure. First one is external gamma exposure that directly affect the human body and the second one is internal exposure that we take them into our bodies through food, water and air breathing. Radon (^{222}Rn) and thoron (^{220}Rn), the gaseous daughter products of ^{238}U and ^{232}Th, respectively, contribute to internal exposure. In addition, some radionuclides such as (^{14}C, ^{40}K and ^{226}Ra) exist in our tissue and organs, such as blood or bones (USNRC, 2019).

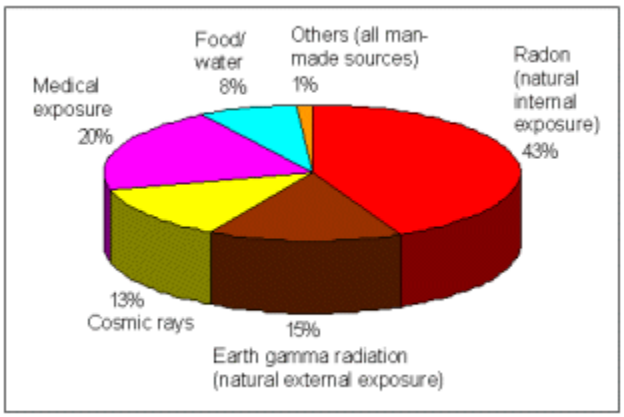

Figure 1.1 Sources and distribution of average radiation exposure to the World population (WHO, 2019).

About one-half of the effective dose from natural sources is estimated to be delivered by inhalation of the short-lived radon decay products (UNSCEAR, 2000). Radon is a naturally occurring radioactive gas released in rock, soil and water. According to EPA, radon gas is odorless and invisible and the only way to know is to test for it. Breathing radon can increase the risk of lung cancer. In the 19^{th} century, about 75% of the miners died from lung cancer. After the identification of radon by Marie and Pierre Curie, the first measurements in the mines were made in 1901. After more precise measurements, a correlation between radon exposure and lung cancer was suggested in the 1920s. This hypothesis was confirmed in 1940 (Swedjemark G.A. 1998).

Studies performed on populations (cohort) of uranium miners clearly showed the linear relation between exposure to radon and risk of lung cancer. This relation is dependent on the age, time since exposure and duration of exposure According to EPA, radon is the most important reason of lung cancer among non-smokers. EPA estimates that radon causes more than 20,000 deaths from lung cancer each year in the U.S. (Atik Ş, 2014).

Therefore, it is interesting to investigate the radioactivity content of Beylikova-Sivrihisar complex ore site. This is because this mining area has an apparent reserve of 53 million tons complex ore which consists of 37.44% fluorite, 31.04%barite, %0.217thorium oxide and 3.14%rare earth oxides (Kayabalı İ. MTA 1986; Kaplan H. MTA 1977)

The main objective of this thesis is to determine a radioactivity content of complex ore Beylikova-Sivrihisar in Eskişehir by employing a high resolution gamma-ray spectrometry, and then to estimate the possible external and internal gamma dose levels to mining workers before starting an ore mining operation.

2. THEORETICAL

2.1 Fundamentals of Radioactivity and Radiation

Radioactivity is the process through which nuclei spontaneously emit subatomic particles. Three types of radiation as known that are α particles, βetas and γ-rays. Then several other particles such as neutrons, protons, positrons and neutrinos were also discovered. When nuclei emit subatomic particles, their configuration, state, and even identity may change. Except for γ-decay, in which the nucleus retains its identity (mass and atomic number are constant), all other decays transform the nucleus into a totally different one. This process is called radioactive decay (Ahmed S.N. 2007).

Radioactive decay is a random process and can simply be explain the Poisson distribution. What this essentially means is that the rate of decay of radioactive nuclei in a large sample depends only on the number of decaying nuclei in the sample by the following decay law:

$$\frac{dN}{dt} = -\lambda_d N \tag{2.1}$$

Where dN represents the number of radioactive nuclei in the sample in the time interval dt. λ_d is a proportionality constant generally referred as decay constant. The solution of Eq. (2.1) gives the number N of the radioactive atoms present in the sample at time t:

$$N = N_0 e^{-\lambda_d t} \tag{2.2}$$

Where N_0 represents the number of radioactive atoms in the sample at t = 0.

Then the rate of decay of a nuclide is called the activity, A, as follows:

$$A = A_0 e^{-\lambda_d t} \tag{2.3}$$

The half-life ($t_{1/2}$) of a radionuclide is used for denoting the time that decreasing the initial atoms numbers to half value. So half-life is inversely proportional to the decay constant,

$$t_{\frac{1}{2}} = \frac{\ln_2}{\lambda} \tag{2.4}$$

and from this definition, the mean life of a radioactive isotope can be calculated since this scale is also directly related with the decay constant.

$$\tau = \frac{1}{\lambda} \tag{2.5}$$

2.2 Naturel Decay Series

Some radioactive elements such as thorium; ^{232}Th, have a very long half-life, (14.05×10^9 years) according to the age of the world, and radioactivity can still be observed today. The source of natural radioactivity in our environment is based on some of radionuclides such as ^{238}U, ^{235}U, ^{232}Th and ^{40}K.

Today we know that most of the natural radioactive elements are composed of very heavy isotopes. These are generally unstable to decay by emitting alpha (α), beta (β^-), positron (β^+), electron capture (EC) or spontaneous fission (SF) products. The final result of all these decays is to reduce the mass number (A) and the atomic number (Z) until it reaches the stable nucleus (Knoll G. F. 2000).

Table 2.1 Decay series of Uranium (^{238}U) (Anonymous 2019-a)

Isotope	Half-life	Decay
^{238}U	$4.49x10^9$ y	α
^{234}Th	24.1 d	β^-
^{234}Pa	1.17 min	β^-
^{234}U	$2.45x10^5$ y	α
^{230}Th	$7.54x10^4$ y	α
^{226}Ra	1602 y	α
^{222}Rn	3.82 d	α
^{218}Po	3.05 min	α
^{214}Pb	26.8 min	β^-
^{214}Bi	19.8 min	β^-
^{214}Po	0.1643 sec	α
^{210}Pb	22.3 y	β^-
^{210}Bi	5.01 d	β^-
^{210}Po	138.4 d	α
^{206}Pb	stable	-

Uranium occurs in the nature as three major isotopes, ^{238}U, ^{235}U and ^{234}U, with relative abundances of 99.27%, 0.72% and 0.0055%, respectively. ^{238}U decays to stable structure that ^{206}Pb at a half-life period of $4.468x10^9$ years. ^{235}U ($7.038x10^8$ years) is also known as in other words Actinium series which decays to other isotopes until stable ^{207}Pb.

Table 2.2 Decay series of Actinium (^{235}U) (Anonymous 2019-a)

Isotope	Half-life	Decay
^{235}U	$7.04x10^8$ y	α
^{231}Th	25.52 h	β^-
^{231}Pa	$3.27x10^4$ y	α
^{227}Ac	21.77 y	β^-
^{227}Th	18.68 d	α
^{223}Ta	11.43 d	α
^{219}Rn	3.96 sec	α
^{215}Po	1.78 msec	α
^{211}Pb	36.1 min	β^-
^{211}Bi	2.14 min	α
^{207}Tl	4.77 min	β^-
^{207}Pb	stable	-

Thorium occurs in the nature as the isotopes, ^{227}Th, ^{228}Th, ^{229}Th, ^{230}Th, ^{231}Th, ^{232}Th and ^{234}Th, most of them have short life time. Thorium consist almost to 100% abundance in weight and it is a very long-lived isotope ^{232}Th (14.05x 10^9 years). ^{232}Th decay series disintegrate until reaches a stable ^{208}Pb isotope.

Table 2.3 Decay series of Thorium (^{232}Th) (Anonymous 2019-a)

Isotope	Half-life	Decay
^{232}Th	1.41x10^{10} y	α
^{228}Ra	5.7 y	β^-
^{228}Ac	6.13 h	β^-
^{228}Th	1.91 y	α
^{224}Ra	3.64 d	α
^{220}Rn	55 sec	α
^{216}Po	0.158 sec	α
^{212}Pb	10.64 h	β^-
^{212}Bi	60.5 min	β^- ,α
^{212}Po	3.04x10^{-5} sec	α
^{208}Tl	3.10 min	β^-
^{208}Pb	Stable	-

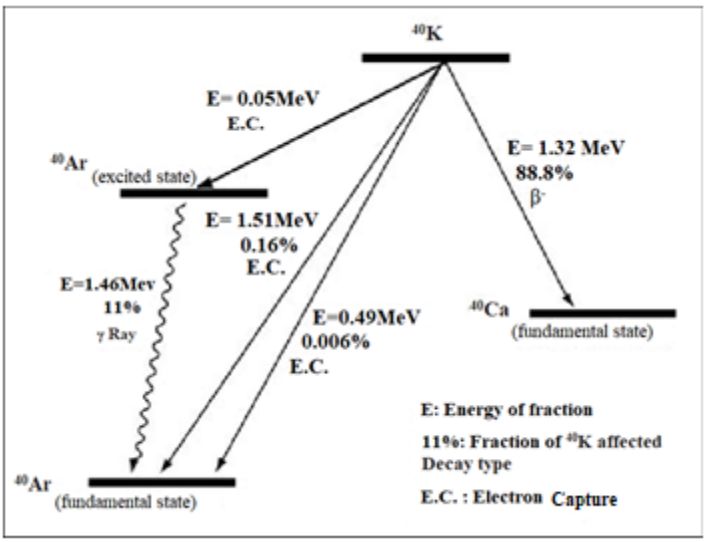

Figure 2.1 Decay schema of Potassium (^{40}K) (Gillot, P.Y. etc, 2006).

Potassium occurs in the nature as three isotopes, ^{39}K, ^{40}K and ^{41}K, with relative abundances of 93.258%, 0.0117% and 6.73%, respectively. However ^{40}K is radioactive and decays to produce ^{40}Ar at a half-life period of $1.25x10^{9}$ years (Gillot, P.Y. etc, 2006).

2.3 Gamma Ray Spectrometry

In gamma spectrometry, firstly gamma rays reach the detector crystal and these gamma rays creating electrical pulses directly proportional with their energies. These pulses are processed in a preamplifier and amplifier, then digital signal obtained from analog to digital converter. The multi-channel analyzer is the system where these signals become the spectrum and this acquired spectrum is analyzed using a suitable algorithm in a software working on the computer. A typical schematic diagram of a gamma-ray spectroscopy system is shown in Figure 2.2

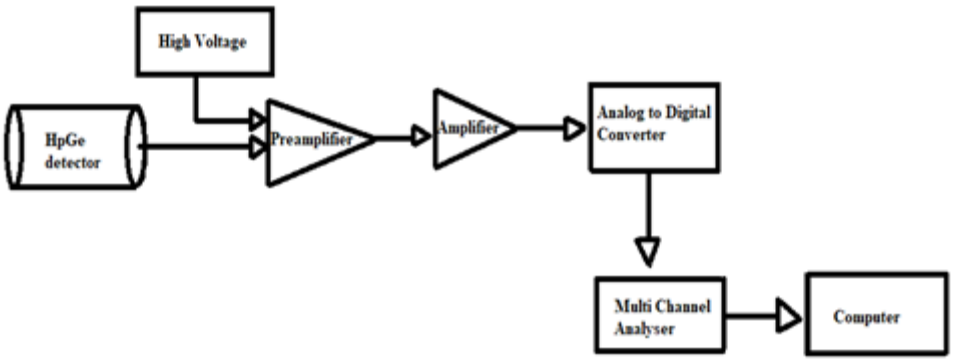

Figure 2.2 Gamma spectroscopy system blog diagram

The net area under each of the observed photopeak in the spectrum, give us total number of gamma transmitting all its energy to the detector, depending on detector efficiency (Debertin K. etc. 1988). The main component of this system is the detector used. In this thesis, a high resolution high purity Germanium (HpGe) is used for the radioactivity measurement.

2.3.1 Main features of HpGe detectors

A high-purity germanium detector is one of the semiconductor detectors that has suitable for gamma-ray measurements due to some distinctive features. Since semiconductors are basically crystalline solids in which atoms are held together by covalent bonds. They are called semiconductors because their electrical conduction properties lie between those of insulators and conductors.

In recent years, advances on purification techniques of Ge crystal have lead to produce the larger volume, high-purity Ge detectors (HpGe) crystals which have recently been made available in the gamma-ray spectrometry. The distinctive features such as a high resolution and a wide dynamic range make them highly suitable for spectroscopic purposes. As shown in Figure 2.3, HpGe detectors can be designed as p-type or n-type or planar and coaxial, well-type as crystal configurations. The advantage of the coaxial geometry is the provision of the large active volume required in the gamma spectrometer. The coaxial HpGe detectors are also manufactured as well type. In this type crystal geometry, the welding is almost completely wrapped by the crystal and the efficiency of the detection increases this enables us to measure small size samples by placing the source in this well. (Debertin K. etc. 1988).

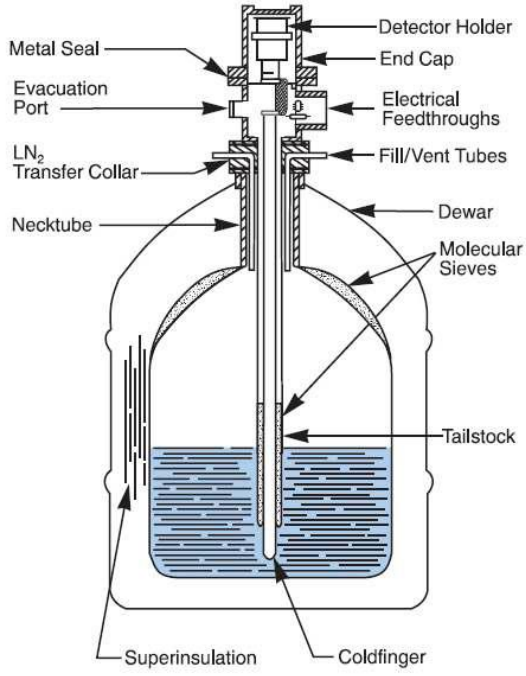

Figure 2.3 Structural diagram of HpGe detector (Reguigui N. 2006)

2.4 Net Photopeak Area Determination

If the total count of the photopeak is indicated by N, then it is simply calculated by summing the counts in each channel.

$$N = \sum_{i=l}^{u} y_i \tag{2.6}$$

Where, y is the count in any i-th channel, *l* and *u* show the channel number in the left and right ends of the photopeak.

Net photopeak area (count) Np refers to counts obtained from photoelectric interactions and it is calculated by subtracting Compton continuum C_{PT} from total count N, which is caused by Compton continuum in the interested energy (Yücel H. etc. 2009).

$$N_P = N - C_{PT} \tag{2.7}$$

2.4.1 Determination of Compton continuum

Compton continuum is determined commonly employing either simple a linear function or more complex stepwise function. In this thesis, the linear function method is preferred if there is no slope at the bottom of the Compton plateau, otherwise the other method can also use. Compton continuum, C_{PT}, calculated from this equation.

$$C_{PT} = \left(\frac{p}{2n}\right)(C_1 + C_2) \tag{2.8}$$

Where, *p* is the number of channels under the photopeak, n is the number of Compton continuity channels on the right and left of the photopeak, C_1 is total counts in the left side of the photopeak, and C_2 is the total counts in the right side of the photopeak (Yücel 2008).

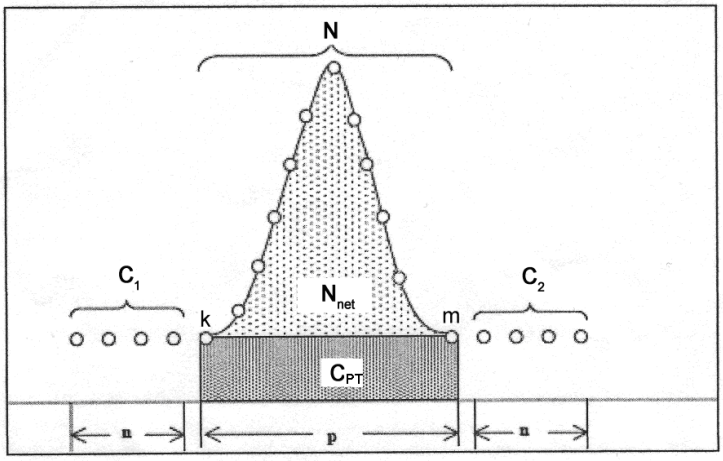

Figure 2.4 Compton continuity determination useing linear function

(Genie 2000 Handbook)

In case of step function for the determination of Compton continuum under the photopeak, we should check whether there is a slope at the bottom of the Compton plateau or not. Compton continuum C_{PT}, is calculated as follows (Yücel 2008).

$$C_{PT} = \sum_{i=k}^{p} \left(\frac{pC_1}{n} + \frac{C_2 - C_1}{nN} \sum_{j=k}^{i} y_j \right) \tag{2.9}$$

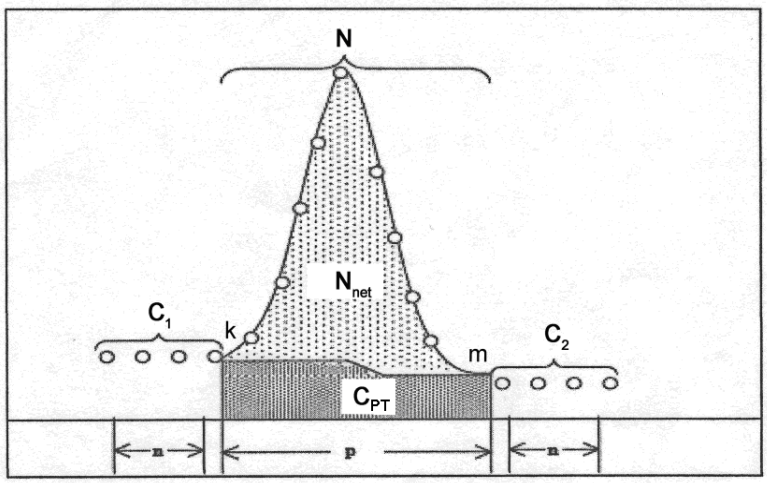

Figure 2.5 Compton continuity determination by using step function

(Genie 2000 Handbook)

2.4.2 Background subtraction from photopeak counts

When there is no source in the detector, the natural background spectrum of the counting system should be measured. The natural background area (N_B) should be determined for interested photopeak from the natural background spectrum. This value must be subtracted from the photopeak area in order to find the real net count (Yücel H. etc. 2017).

$$N_{Net} = N - C_{PT} - N_B \tag{2.10}$$

2.5 Detection Efficiency

In gamma spectroscopy, total efficiency (ε_t) means that ratio of gamma rays counted by detector (N_d) to the gamma rays emitted from the source (N_s), and its represent by this equation;

$$\varepsilon_t = \frac{N_d}{N_s} \tag{2.11}$$

Other useful expression for gamma spectroscopy is photopeak efficiency (ε_f) which is ratio of gamma rays counted under the photopeak area (N_f) to the gamma rays emitted from the source (N_s), and it is represented by this equation (Yücel H. 2008);

$$\varepsilon_f = \frac{N_f}{N_s} \tag{2.12}$$

2.6 Absolute Activity Measurement Method

The two well-known activity determination method is that one is standard comparison and the other is absolute (direct) measurement method. The first one necessitates the suitable matrix similar to the real sample but this is not always possible. Therefore, the second method is more commonly employed in gamma-ray spectrometry. For using absolute (direct) activity determination method, the efficiency at a given measurement geometry must be the same with that of the activity measurement geometry. After this condition is met, we can find the activity of interested radionuclide by the following equation;

$$C_x = \frac{\left[\frac{N_p^x}{t_x} - \frac{N_B}{t_B}\right]}{\varepsilon_f(E) \cdot f_\gamma(E) \cdot \mathrm{m}} \tag{2.13}$$

Where, N^x_p/t_x denotes the net count rate (photopeak count in cps), N_B/t_B denotes the natural background count rate (in cps), $f_\gamma(E)$ is possibility of gamma emitting for this energy value, $\varepsilon_f(E)$ is photopeak efficiency for interested energy and m is mass of sample (Debertin K. etc. 1988).

2.7 Correction Factors for Accurate Activity Determination

2.7.1 Radioactive decay correction factor

Activity of radioactive sample is decreasing day by day because of this reason it should be used appropriate correction factor that;

$$K_b = \mathrm{e}^{\left(-\frac{\ln 2 \cdot \Delta t}{t_{1/2}}\right)} \tag{2.14}$$

In this equation, Δt express the time from collection of samples to the time of measurement (sec) and $t_{1/2}$ is half-life of the radionuclide (sec). For very long half-life radionuclides $K_b \cong 1$ is acceptable.

2.7.2 Measurement time correction factor

As it is known the time during which the system remains active (live time) is used as the counting time but we also know that real time is different from the live time because of the dead time of the detector. In order to take this into account, a correction factor is calculated based on the actual time at the time of measurement.

$$K_c = \frac{t_{1/2}}{\ln 2 \cdot t_r}\left(1 - e^{\left(-\frac{\ln 2 \cdot t_r}{t_{1/2}}\right)}\right) \tag{2.15}$$

In this equation, t_r is real time by during the measurement (sec), for very long half-life radionuclides $K_c \cong 1$ is acceptable (Yücel H. 2008).

2.7.3 Random summing correction factor

Random summing (pulse pileup effect) is a result of simultaneous detection of two consecutive pulses of the same or different energy, within the resolving time of the spectrometer. At higher counting rates more pulses are quantitatively affected. Therefore, random summing correction factor is required if dead time value is more than %10.

$$K_r = e^{(2 \cdot R \cdot \tau)} \tag{2.16}$$

In this equation, R is total count rate (integral) and τ is resolving time of the counting system.

2.7.4 Gamma-ray self-absorption correction factor

Especially in low energy gamma-rays, gamma-ray self-absorption correction factor should be used to correct the losses in peak area due to mainly sample matrix and its density. For the calculation of the self-absorption factor the chemical composition of the samples must be known. Sample mass absorption coefficient due its composition can expressed as follows;

$$\mu_k = \sum_{i=l}^{n} w_i \mu_i \tag{2.17}$$

In this equation, μ_i is mass absorption coefficient of each component and w_i is weighting factor of each component in sample.

Self-absorption coefficient can be calculated for cylindrical geometry at a given distance from the endcap as;

$$K_0 = \frac{\mu_k \cdot \rho \cdot d}{1 - e^{-\mu_k \cdot \rho \cdot d}} \tag{2.18}$$

Where, μ_k is mass absorption coefficient of composition and ρ is density of composition and d is thickness of the sample (Yücel H. 2008).

2.8 Uncertainty Estimation

2.8.1 Uncertainty of activity

The uncertainty of activity value consists of mainly the uncertainties in the net count rate of the photopeak (including background subtraction, the probability of gamma emission the efficiency of photopeak, the amount of sample and the correction factors, and another systematic ones (type B) such as filling level of the container, dry mass, etc.

$$u(A) = A \cdot \sqrt{\left(\frac{u(N_p)}{N_p}\right)^2 + \left(\frac{u(\varepsilon)}{\varepsilon}\right)^2 + \left(\frac{u(f_\gamma)}{f_\gamma}\right)^2 + \left(\frac{u(m)}{m}\right)^2 + \left(\frac{u(K)}{K}\right)^2} \qquad (2.19)$$

Where, A is the activity of the sample, Np is net count of photopeak that Compton continuity and natural fund correction made, ε is photopeak efficiency, u(ε) is uncertainty of the photopeak efficiency, f is gamma emitting probability u(fγ) is uncertainty of gamma emitting probability m is amount of the standard and u(m) is uncertainty of standard quantity, K is composition of correction factors and u(K) is correction uncertainty (Yücel H. 2008).

3. MATERIALS AND METHODS

3.1. Description of Study Area

Eskişehir-Beylikova region is located east side of the Eskisehir and total area is 17.2 km² and this area is marked as seven region considering the soil characteristics by Etimaden corporation. These are Devebağırtan, Koca devebağırtan, Yaylabaşı, Küçükhöyüklü, Canavarini, Kocayayla and Köyyeri. Apparent complex reserves is estimated to be 53 million tons consisting mainly barite and fluorite but it contains thorium oxide (amounts to 380.000 tons), rare earth elements oxides (Anonymous 2017). According to the official permission of Etimaden dated 08.08.2018 and number 50894663-130.01, we collected samples from seven section under supervising a geology expert of Etimaden corporation on 08/11/2018. We collected the sixty samples from five different fixed locations the sampling locations are also indicated in Figure 3.2 and positions of sample locations are defined by GPS.

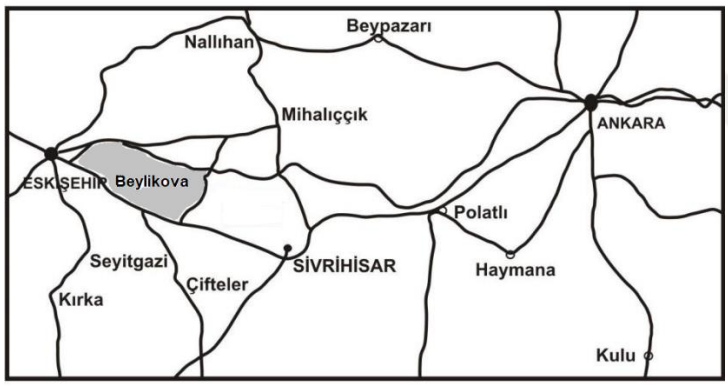

Figure 3.1 Rare earth elements ore site

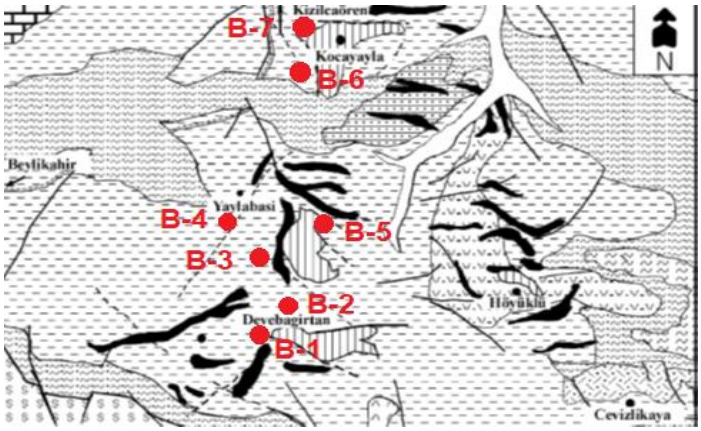

Figure 3.2 Beylikova rare earth elements section map

Gallery (B1) coordinates:

- 36-358-698 East
- 438-41-52 North
- 1208 Z Height

3.2 Sampling and Sample Preparation

In sampling procedure, the special tools are used in this site and the collected samples are packed in bags and labeled them. In the sample preparation in the laboratory, firstly we dried ore, crushed and milled and powdered samples were homogenized using a ring grinder (Vommak brand), thus providing grain size of less than 1 μm. After all these processes we sieved the samples with Retsch brand AS-300 sieve and this samples weighed with a balance (And brand) which has a precision scale providing an accuracy of±0.1 mg.

Figure 3.3 Jaw crusher

Figure 3.4 Ring grinder

Figure 3.5 Sieve

Figure 3.6 Scales

These samples crushed and sieved then we used the silicon, paraffin and sealed band for sealing this container. All these sealed containers labeled with preparation dates and weights of the samples for later use.

Figure 3.7 Marinelli beakers top and bottom view

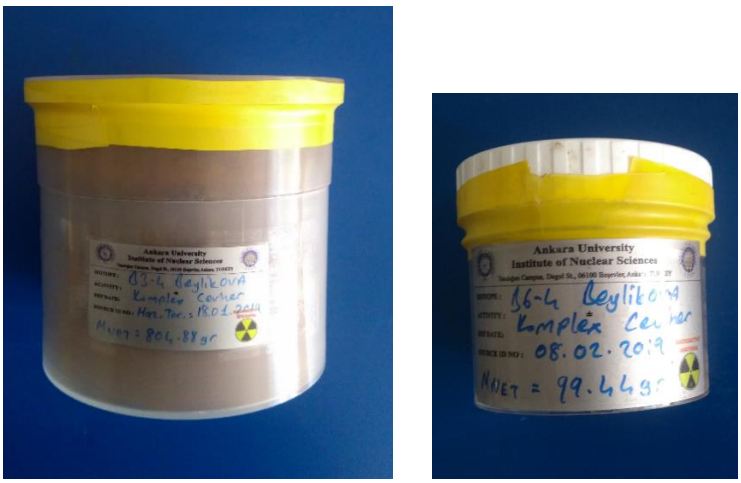

Figure 3.8 Filled up Marinelli and Cylinder containers

3.3 Gamma Spectroscopy System

Measurements were made with an n- type HpGe detector (ORTEC GMX70P4-S). The detector specifications are given in Table 3.1 The detector is armored with the ORTEC Model PB armor to minimize the impact of natural background radiation. A 30 L, double walled (vacuum) liquid nitrogen container was used to cool the detector.

Table 3.1 HpGe detector properties

Detector geometry and crystal type		Close end, coaxial, n-type
Relative efficiency		%78.5
Active volume		218 cm^3
Germanium crystal	Radius	34.95 mm
	Height	82.6 mm
Energy separation power (FWHM)	122 keV (^{57}Co)	1.16 keV
	1332.5 keV (^{60}Co)	2.01 keV
Peak-Compton ratio	1332.5 keV (^{60}Co)	75:1

Gamma spectrometry system also contains Ortec 138 EMI high voltage power supply through a DIM module, an Ortec A257N resistance feedback preamplifier and spectroscopic amplifier. The spectrum is controlled by the Gamma Vision gamma spectroscopy software, with a 16K converting multiport multichannel analyzer.

In this thesis, the Gespecor computer simulation program (Version 3.2) is used to calculate efficiency, true coincidence and self-absorption factors because there is no suitable standard similar to samples. In the simulation model, all features are described taking into account all geometric parameters and material properties. To do this, some detector specifications about our design that detector types and physical parameters, shielding materials, sample geometry and others are given in n Table 3.2. Then emission probability of gamma ray, coincidence factor, and linear attenuation coefficient and detector efficiency are reported after calculation.

3.3.1 Preparation of data in for sample-detector simulation

Table 3.2 Detector related file input data

Detector type:	HpGe	**Detector holder**	Aluminum
Crystal radius (cm):	3.495	Face thickness (cm):	0.005
Crystal length (cm):	8.26	Side thickness (cm):	0.076
Inner contact radius (cm):	0.46	Density (g/cm^3):	2.7
Inner contact length (cm):	7.38	**End Cap**	Beryllium
Thickness of dead layer		Diameter (cm):	8.26
Active face (cm):	0.0003	Window thickness (cm):	0.0508
Side face (cm):	0.0003	Density (g/cm^3):	1.848
Distance from the active face to entrance window:	0.40	**End Cap Side Material:**	Aluminum
		Side thickness (cm):	0.10
		Density (g/cm^3):	2.7

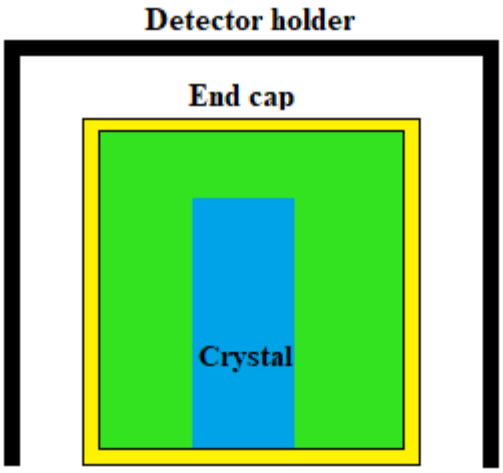

Figure 3.9 Detector configuration used in simulation

Table 3.3 Geometry related file input data

Sample geometry type:	Marinelli
Sample inner radius (cm):	4.68
Sample inner height (cm):	7.6
Sample outer radius (cm):	6.1
Sample outer height (cm):	9.2
Container wall thickness (cm):	0.5
Material type:	Polypropylene
Density (g/cm^3):	0.9
Distance from the end cap to the container bottom (cm):	0.05

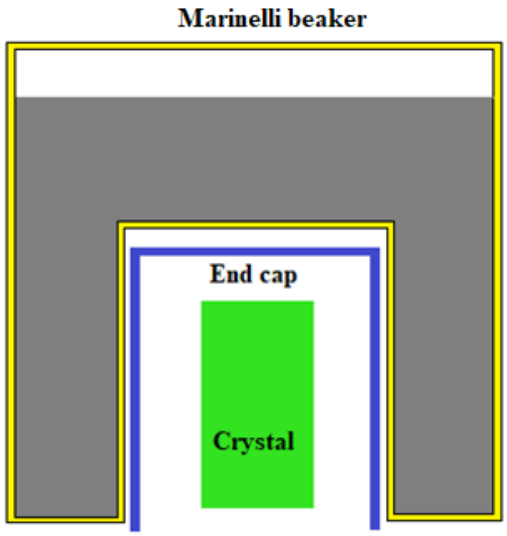

Figure 3.10 Geometry configuration used in simulation

3.3.2 Lead shield related file input

Table 3.4 Geometry file input data

Shield material type:	Lead
Shield inner radius (cm):	14.0
Shield inner height (cm):	40.0
Shield outer radius (cm):	25.5
Shield outer height (cm):	63.0
Density (g/cm^3):	11.35
Distance from the end cap to inner top of shield (cm):	9.0

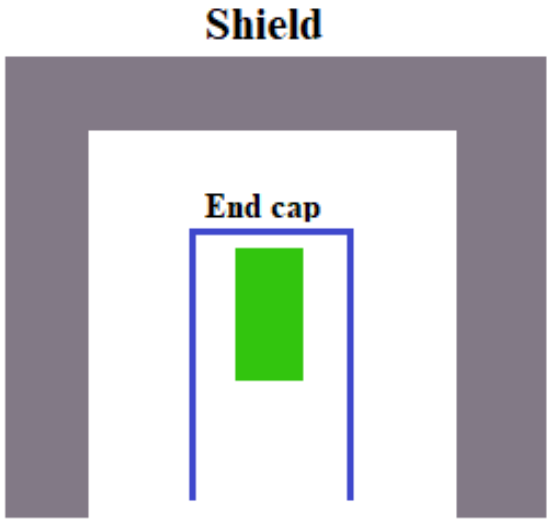

Figure 3.11 Shield geometry used in simulation

Figure 3.12 A photograph of the HpGe Detector used in experiments

3.4 Background Spectrum Measurement

The natural background spectrum of the laboratory was measured without any source around the detector. These measurements were repeated three times and averaged the obtained count rates. Each of the measurements was lasted for at least three days to get sufficient statistics at different sessions.

3.5 Gamma-ray Self Absorption Coefficient Calculation

In order to calculate the gamma ray self-absorption correction factor, the chemical composition of the samples was calculated with XRF method. After the chemical element composition is found, mass reduction coefficients were calculated using the NIST XCOM database.

3.6 Efficiency Calibration for Relevant Peaks

In order to obtain the detection efficiency, we use the Gespecor data, because we use the direct activity measurement method so we did not use any references material which is not available.

Table 3.5 The calculated data for efficiency and self-absorption factors

Radionuclide	**Energy(keV)**	f_γ **(%)**	**Fcoi**	**μ**	**ε**
^{228}Ac (^{232}Th)	338.32	11.4	0.959	0.113	0.056
^{228}Ac (^{232}Th)	911.196	26.2	0.973	0.065	0.031
^{208}Tl (^{232}Th)	583.187	30.6	0.844	0.082	0.040
^{208}Tl (^{232}Th)	860.56	4.3	0.936	0.067	0.031
^{226}Ra	186.21	3.6	1.0	0.200	0.068
^{214}Pb (^{226}Ra)	295.224	18.4	1.0	0.125	0.060
^{214}Pb (^{226}Ra)	351.932	35.6	0.999	0.110	0.054
^{214}Bi (^{226}Ra)	609.312	45.5	0.867	0.080	0.039
^{214}Bi (^{226}Ra)	1120.287	14.9	0.857	0.058	0.027
^{234m}Pa (^{238}U)	1001.03	0.8	1.0	0.062	0.028
^{40}K	1460.822	10.6	1.0	0.051	0.023

3.7 Activity Measurement of Samples

Activity measurement results were obtained by using absolute activity measurement method which is explained in section 2.6 The samples were measured for two to three days to provide sufficient counting statistics. Before making activity measurement we made the spectral interference correction to the peak area for determining more accurate activity value (Yücel H. etc. 2009, Akkaya G. 2011)

The main radionuclide of uranium decay series that ^{238}U, are emitting very weak gamma rays which are difficult to measure in 49.5 keV (%0.064) and 113.5 keV (%0.0102) energy (Yücel H. etc. 1998). Therefore, the activity of ^{238}U is assumed to be in balance with product nuclides ^{234}Th (24.1 days) and ^{234m}Pa (1.17 minutes) (Huy N.Q.etc. 2004).

^{234m}Pa has only the most severe peak at 1001 keV(%0.842) energy and this peak have less self-absorption coefficient value compared to that of 63.3 keV energy peak which is emitted by ^{234}Th daughters so using 1001 keV energy peak is giving more accurate ^{238}U activity.

In uranium series high probability gamma rays is released from ^{214}Pb and ^{214}Bi nuclides. Depending on their short half-life, these two nuclides reach equilibrium with ^{226}Ra in a closed system less than a month. So we use these two nuclides and also ^{226}Ra (which is released 186.2 keV (%3.64) gamma rays) for determining ^{226}Ra activity. Gamma rays of the ^{214}Pb nuclides are the most severe at 295.2 keV (%18.4) and 351.9 keV (%35.6) and also gamma rays of the ^{214}Bi nuclides are the most severe at 609.3 keV (%45.5) and 1120.2 keV (%14.9) (Anonymous, 2019-c). ^{226}Ra activity determined by taking the arithmetic mean of its own peak (186.2 keV) and decay products ^{214}Pb (295.2 keV and 351.9 keV) peaks and ^{214}Bi (609.3 keV and 1120.2 keV) peaks (Yücel H. etc. 2017).

$$N_p[186.2\ \text{keV},\ ^{226}Ra] = \frac{[I_\gamma \cdot \varepsilon_p \cdot F_{COI} \cdot F_s]_{186.2\ keV}}{[I_\gamma \cdot \varepsilon_p \cdot F_{COI} \cdot F_s]_{295.2\ keV}}\ x\ N_p[295.2\ \text{keV},\ ^{214}Pb] \qquad (3.1)$$

The nuclides with the most interest in environmental studies in the thorium series were ^{228}Ra (5.75 years) and ^{228}Th (1.9131 years). In the case of equilibrium, ^{228}Ra product nuclide ^{228}Ac and ^{228}Th product nuclides can be determined from ^{208}Tl. The most severe gamma rays of ^{228}Ac are 338.4 keV (%11.40), 911.1 keV (%26.2) and 968.9 keV (%16.23). The most severe gamma energy of ^{208}Tl is 583.1 keV (%30.62) and 860.5 keV (%4.51). ^{232}Th activity was calculated by taking the arithmetic mean of the related photopeak of the decay products ^{228}Ac (338.4 keV and 911.1 keV) peaks and ^{208}Tl (583.1 keV and 860.5 keV) peaks.

Potassium activity is measured from photopeak energy of 1460.8 keV of ^{40}K nuclide. In most cases, photopeak at 1460.8 keV is a peak of ^{40}K and ^{228}Ac. Because ^{228}Ac nuclides emitted 1459.2 keV energy (%1) gamma rays (Reus and Westmeier 1983). So this measurement corrected by spectral interference method for the contribution from ^{228}Ac nuclide (Yücel H. etc. 2017).

$$N_p[1460.8\ \text{keV},\ ^{40}K] = \frac{[I_\gamma \cdot \varepsilon_p \cdot F_{COI} \cdot F_s]_{1460.8\ keV}}{[I_\gamma \cdot \varepsilon_p \cdot F_{COI} \cdot F_s]_{1459.2\ keV}}\ x\ N_p[1459.2\ \text{keV},\ ^{228}Ac] \qquad (3.2)$$

Table 3.6 Radionuclides used in calculations and their properties

Radionuclide	**Decay Product**	**Gamma-ray Energy (keV)**	f_γ **(%)**
^{238}U	^{234m}Pa	1001.03	0.84
^{226}Ra	^{222}Rn	186.21	3.64
	^{214}Pb	295.224	18.41
		351.932	35.6
	^{214}Bi	609.312	45.49
		1120.287	14.91
^{232}Th	^{228}Ac	338.32	11.4
		911.196	26.2
	^{208}Tl	583.187	30.62
		860.56	4.51
^{40}K	^{40}K	1460.822	10.66

3.8 Quantities Calculated by Using Measured Activity Values

3.8.1 Radium equivalent activity

Radium equivalent activity is used to convert the activity of samples containing different amounts of radium, thorium and potassium in the content.

$$A_{Ra\text{-}eq} = A(^{226}Ra) + 1.43\ A(^{232}Th) + 0.077\ A(^{40}K) \quad (3.3)$$

Radium equivalent activity calculated from this equation. In this equation A (^{226}Ra), A (^{232}Th) and A (^{40}K) are respectively radium, thorium and potassium activity (Bq·kg^{-1}) (Knoll G. F. 2000).

3.8.2 Absorbed dose rate

Uniform distribution of naturally occurring nuclides at a height of 1 m from the ground, absorbed dose rate due to gamma ray is calculated from this equation (Anonymous, 2000).

$$D = 0.462 \times A(^{226}Ra) + 0.621 \times A(^{232}Th) + 0.0417 \times A(^{40}K) \quad (3.4)$$

In this equation A(^{226}Ra), A(^{232}Th) and A(^{40}K) are respectively radium, thorium and potassium activity (Bq·kg^{-1}).

The annual effective dose rate calculation factor is 0.7 Sv/Gy and occupancy factor is 0.2 for outdoor and 0.8 for indoor calculations. (Anonymous, 2000).

$$ED_{out} = D(nGy\ h^{-1})\ \text{x}\ 2000h\ \text{y}^{-1}\ \text{x}\ 0,7\ \text{x}\ \frac{10^3 mSv}{10^9 nGy}\ \text{x}\ 0,2 \tag{3.5}$$

$$ED_{in} = D(nGy\ h^{-1})\ \text{x}\ 1000h\ \text{y}^{-1}\ \text{x}\ 0,7\ \text{x}\ \frac{10^3 mSv}{10^9 nGy}\ \text{x}\ 0,8 \tag{3.6}$$

Due to variability of mining operations area, we calculated annual effective dose rate by not only indoor but also outdoor occupancy factor. Effective dose rate for employees should not exceed 20 mSv per year and averaged over a five-year period not exceed the 50 mSv effective dose rate (ICRP, 1993).

3.8.3 Gamma activity concentration index

Another approach used to calculate the effective dose rate is the calculation of the gamma activity concentration index.

$$I = \left[\frac{A(^{232}Th)}{200} + \frac{A(^{226}Ra)}{300} + \frac{A(^{40}K)}{3000} \right] \tag{3.7}$$

A(^{226}Ra), A(^{232}Th) and A(^{40}K) are the radium, thorium and potassium activities(Bq·kg^{-1}), respectively. In order to ensure that the effective dose rate does not exceed 1 mSv·y^{-1}, gamma activity concentration index should be $I \leq 1$ (Anonymous, 1999).

3.8.4 Health hazard index

The external health hazard index H_{ex} was calculated using the model proposed by Krieger (Khatun M.A. etc. 2018);

$$H_{ex} = \left[\frac{C(^{226}Ra)}{370} + \frac{C(^{232}Th)}{259} + \frac{C(^{40}K)}{4810} \right] \tag{3.8}$$

The H_{ex} index must be less than unity so that the annual effective dose due to radioactivity in the material will be considered safe. In addition to H_{ex} index, inhaled radon and its short-lived progeny also represent a risk to the respiratory organs. Internal exposure to radon and its progeny can be quantified using the index H_{in}, which was estimated by the following expression (Khatun M.A. etc. 2018);

$$H_{in} = \left[\frac{C(^{226}Ra)}{185} + \frac{C(^{232}Th)}{259} + \frac{C(^{40}K)}{4810} \right] \tag{3.9}$$

For the utilization of a working area to be considered safe, H_{in} must be less than unity (Krieger R. 1981).

4. RESULTS

4.1 Determination of the Content of Samples

We need the content of the samples for determining some specific qualifications like a self-absorption coefficient, efficiency and gamma emission fraction, so we use the X-ray spectrometric analysis methods (XRF) for determining content of the sample. This method applicable in many different ways and we use the standard comparison method. In this method the characteristic analyze line intensity released from the sample is compared with the standard which has the same or close matrix concentration. By this way we obtained the information about the content of the sample.

Table 4.1 Composition and percentage of the samples determined by XRF method

Composition	**Percentage**
$BaSO_4$	31.04
CaF_2	37.44
ThO_2	0.2
Y_2O_3	3.14
SiO_2	5.1
Fe_2O_3	7.92
MnO_2	0.62
Al_2O_3	7.37
$CaCO_3$	2.67
K_2CO_3	2.95
MgO	2.04
U_3O_8	0.021

4.2 Background Spectrum

In the gamma counting system, as described in Section 3.5, the natural background spectrum of the laboratory was measured without any source around the detector.

Table 4.2 Count rates of photopeak observed in the natural background spectrum

Radionuclide	Energy (keV)	Uncertainty (%)	Count Rate (Count/sec)
^{228}Ac	338.32	20.47	0.001712
^{228}Ac	991.196	12.56	0.002143
^{208}Tl	583.187	11.54	0.003217
^{208}Tl	860.56	2.54	0.0000606
^{226}Ra	186.21	3.55	0.020834
^{214}Pb	295.224	5.51	0.013853
^{214}Pb	351.932	3.63	0.007155
^{214}Bi	609.312	4.17	0.01148
^{214}Bi	1120.287	7.82	0.010063
^{234m}Pa	1001.03	17.46	0.003399
^{40}K	1460.822	5.25	0.018741

4.3 Gamma-Ray Self-Absorption Correction Factors

We can obtain two different gamma-ray self-absorption correction factors. One of them is also calculating by using material specific qualifications that explained in equation 2.21 and the second one is determined by taking the help of the computer program of Gespecor. We use both of this two method and we determine two different K_0 value but in this study we used the Gespecor results, because first calculation contains many different uncertainties which are due to computational characteristics.

Table 4.3 Gamma-ray self-absorption correction factors

Energy (keV)	**K_0**	**K_0 (Gespecor)**
338.32	1.11	1.23
991.196	1.06	1.13
583.187	1.08	1.17
860.56	1.06	1.13
186.21	1.20	1.41
295.224	1.12	1.25
351.932	1.11	1.22
609.312	1.08	1.16
1120.287	1.06	1.12
1001.03	1.06	1.12
1460.822	1.05	1.10

4.4 Activity Measurement of the Samples

We have classified our samples according to its regions.

Table 4.4 Sample activities calculated with gamma-ray self-absorption factors

Sample Name	^{238}U(Bq·kg^{-1})	^{232}Th(Bq·kg^{-1})	^{226}Ra(Bq·kg^{-1})	^{40}K(Bq·kg^{-1})
B1-1	1443 ± 40	3723 ± 9	1348 ± 4	116 ± 2
B1-2	1929 ± 45	4801 ± 11	1787 ± 5	141 ± 2
B1-3	3278 ± 20	1299 ± 5	3457 ± 6	57 ± 1
B1-4	1480 ± 19	1427 ± 5	1365 ± 2	145 ± 3
B1-5	1771 ± 29	4404 ± 8	1587 ± 3	149 ± 1
B1-6	4793 ± 54	1284 ± 7	6030 ± 10	40 ± 1.5
B1-7	2950 ± 38	1197 ± 5	3044 ± 6	43 ± 1.5
B1-8	2680 ± 40	2646 ± 7	2645 ± 6	86 ± 2
B1-9	2516 ± 29	3707 ± 8	2450 ± 5	124 ± 1
B1-10	2253 ± 14	3520 ± 6	2149 ± 3	110 ± 1
B1-11	1695 ± 24	3162 ± 7	1560 ± 4	89 ± 1
B1-12	3444 ± 45	3690 ± 9	2926 ± 6	112 ± 2
B1-13	2151 ± 29	4829 ± 9	1920 ± 4	150 ± 1
B1-14	1819 ± 34	4459 ± 10	1684 ± 4	147 ± 2
B1-15	1940 ± 20	2038 ± 5	1736 ± 3	116 ± 1
B1-16	3414 ± 44	2061 ± 7	3229 ± 6	107 ± 2
B1-17	1915 ± 32	4860 ± 10	1701 ± 4	151 ± 1
B1-18	2276 ± 27	5643 ± 11	2084 ± 4	170 ± 1
B1-19	2072 ± 23	1750 ± 5	2668 ± 5	57 ± 1
B1-20	3237 ± 43	2985 ± 8	3132 ± 6	110 ± 1.5

Table 4.5 Sample activities calculated with gamma-ray self-absorption factors

Sample Name	**^{238}U(Bq·kg^{-1})**	**^{232}Th(Bq·kg^{-1})**	**^{226}Ra(Bq·kg^{-1})**	**^{40}K(Bq·kg^{-1})**
B1-21	1749 ± 14	2434 ± 5	1554 ± 5	149 ± 1
B1-22	2449 ± 35	3066 ± 7	2470 ± 8	102 ± 2
B1-23	3090 ± 38	1943 ± 5	2992 ± 6	60 ± 2
B1-24	1960 ± 37	3954 ± 9	1763 ± 5	142 ± 2
B1-25	1912 ± 49	3943 ± 11	1918 ± 6	134 ± 2
B1-26	2263 ± 52	3970 ± 11	2123 ± 6	147 ± 2
B1-27	2151 ± 16	4265 ± 6	2051 ± 3	124 ± 1
B1-28	2906 ± 36	5817 ± 11	2502 ± 8	172 ± 2
B1-29	2127 ± 33	3534 ± 9	2136 ± 4	140 ± 2
B1-30	1915 ± 16	4500 ± 7	1720 ± 3	141 ± 1
B1-31	2696 ± 64	5872 ± 15	2252 ± 7	181 ± 2
B1-32	2079 ± 35	4051 ± 9	2036 ± 5	135 ± 2
B1-33	2674 ± 62	6049 ± 15	2314 ± 6	168 ± 2
B1-34	2103 ± 30	5009 ± 9	2018 ± 4	160 ± 1
B1-35	2077 ± 61	5034 ± 12	2029 ± 6	152 ± 3
B2-1	4228 ± 22	5463 ± 8	4580 ± 7	158 ± 1
B2-2	3225 ± 30	4797 ± 8	3047 ± 5	184 ± 1
B2-3	4420 ± 17	1543 ± 4	4531 ± 6	44 ± 0.5
B2-4	4399 ± 73	4406 ± 13	3804 ± 9	156 ± 3
B3-1	948 ± 35	6203 ± 12	426 ± 2	255 ± 1

Table 4.6 Sample activities calculated with gamma-ray self-absorption factors

Sample Name	**^{238}U(Bq·kg^{-1})**	**^{232}Th(Bq·kg^{-1})**	**^{226}Ra(Bq·kg^{-1})**	**^{40}K(Bq·kg^{-1})**
B3-2	462 ± 43	2514 ± 7	319 ± 1	1057 ± 3
B3-3	655 ± 30	5240 ± 10	439 ± 2	611 ± 2
B3-4	1046 ± 41	3624 ± 9	903 ± 3	213 ± 2
B4-1	681 ± 25	1959 ± 5	616 ± 2	861 ± 3
B4-2	622 ± 90	3851 ± 7	342 ± 2	1149 ± 5
B4-3	596 ± 41	2535 ± 7	511 ± 2	1072 ± 3
B4-4	226 ± 9	647 ± 2	212 ± 1	1017 ± 2
B5-1	1369 ± 58	6632 ± 16	1087 ± 7	291 ± 3
B5-2	1374 ± 38	3925 ± 10	986 ± 4	120 ± 2
B5-3	1284 ± 59	6615 ± 15	868 ± 4	191 ± 2
B5-4	1489 ± 37	6704 ± 13	964 ± 3	197 ± 1
B6-1	373 ± 16	2258 ± 4	141 ± 1	1024 ± 2
B6-2	331 ± 31	2312 ± 4	111 ± 1	1001 ± 3
B6-3	379 ± 36	2443 ± 7	156 ± 1	1045 ± 4
B6-4	401 ± 39	2307 ± 6	147 ± 2	1057 ± 4
B6-5	276 ± 30	2167 ± 5	98 ± 1	1021 ± 3
B7-1	63 ± 23	431 ± 2	62 ± 0.3	365 ± 1
B7-2	66 ± 8	410 ± 1	52 ± 0.3	372 ± 1
B7-3	82 ± 16	476 ± 2	65 ± 1	356 ± 1
B7-4	80 ± 25	477 ± 2	64 ± 1	372 ± 1

Table 4.7 Absorbed doses, Effective doses and Health hazards of samples

Sample Name	Absorbed Dose (D) (nGy/h)	Effective dose (ED_{in}) ($mSv \cdot y^{-1}$)	Effective dose (ED_{out}) ($mSv \cdot y^{-1}$)	Internal Health Hazard (H_{in})	External Health Hazard (H_{ex})
B1-1	2939 ± 5	1.65 ± 0.3	0.82 ± 0.1	19.3±0.4	15.7±0.3
B1-2	3813 ± 6	2.14 ± 0.3	1.07 ± 0.2	28.2±0.4	23.4±0.4
B1-3	2406 ± 2	1.35 ± 0.1	0.67 ± 0.1	23.7±0.2	14.4±0.1
B1-4	292 ± 2	0.16 ± 0.01	0.08 ± 0.01	2.2±0.1	1.7±0.1
B1-5	3474 ± 4	1.95 ± 0.2	0.97 ± 0.1	25.6±0.3	21.3±0.2
B1-6	3585 ± 5	2.01 ± 0.3	1.0 ± 0.1	37.6±0.4	21.3±0.3
B1-7	2151 ± 3	1.20 ± 0.2	0.6 ± 0.1	21.1±0.3	12.9±0.2
B1-8	2869 ± 5	1.61 ± 0.3	0.8 ± 0.1	24.5±0.4	17.4±0.4
B1-9	3439 ± 3	1.93 ± 0.2	0.96 ± 0.1	27.6±0.3	21.0±0.2
B1-10	3183 ± 2	1.78 ± 0.1	0.89 ±0.15	25.2±0.1	19.4±0.1
B1-11	2688 ± 3	1.51 ± 0.2	0.75 ± 0.1	20.7±0.2	16.4±0.2
B1-12	3648 ± 5	2.04 ± 0.3	1.02 ± 0.1	30.1±0.4	22.2±0.3
B1-13	3892 ± 3	2.18 ± 0.2	1.09 ± 0.1	29.1±0.3	23.9±0.2
B1-14	3553 ± 4	1.99 ± 0.2	0.99 ± 0.1	26.3±0.3	21.8±0.3
B1-15	2072 ± 2	1.16 ± 0.1	0.58 ± 0.1	17.3±0.2	16.2±0.1
B1-16	2776 ± 5	1.55 ± 0.3	0.78 ± 0.1	25.4±0.4	16.7±0.3
B1-17	3810 ± 4	2.13 ± 0.2	1.07 ± 0.1	28.0±0.3	23.4±0.2
B1-18	4474 ± 3	2.51 ± 0.2	1.25 ± 0.1	33.1±0.2	27.5±0.2
B1-19	2322 ± 3	1.30 ± 0.1	0.65 ± 0.1	21.2±0.2	14.0±0.2
B1-20	3305 ± 5	1.85 ± 0.3	0.93 ± 0.1	28.5±0.4	20.0±0.3

Table 4.8 Absorbed doses, Effective doses and Health hazards of samples

Sample Name	Absorbed Dose (D) (nGy/h)	Effective dose (ED_{in}) ($mSv \cdot y^{-1}$)	Effective dose (ED_{out}) ($mSv \cdot y^{-1}$)	Internal Health Hazard (H_{in})	External Health Hazard (H_{ex})
B1-21	2236 ± 3	1.25 ± 0.1	0.63 ± 0.1	17.8±0.2	13.6±0.2
B1-22	3050 ± 5	1.71 ± 0.3	0.85 ± 0.1	25.2±0.4	18.5±0.3
B1-23	2592 ± 4	1.45 ± 0.2	0.73 ± 0.1	23.7±0.3	15.6±0.2
B1-24	3276 ± 5	1.83 ± 0.3	0.92 ± 0.1	24.8±0.3	20.1±0.3
B1-25	3340 ± 6	1.87 ± 0.3	0.94 ± 0.2	25.6±0.5	20.4±0.4
B1-26	3452 ± 6	1.93 ± 0.3	0.97 ± 0.2	26.8±0.5	21.1±0.4
B1-27	3601 ± 2	2.02 ± 0.1	1.01 ± 0.1	27.6±0.1	22.0±0.1
B1-28	4776 ± 5	2.67 ± 0.3	1.34 ± 0.1	36.0±0.3	29.3±0.3
B1-29	3187 ± 4	1.78 ± 0.2	0.89 ± 0.1	25.2±0.3	19.4±0.3
B1-30	3595 ± 2	2.01 ± 0.2	1.01 ± 0.1	26.7±0.1	22.1±0.1
B1-31	4694 ± 8	2.63 ± 0.4	1.31 ± 0.2	34.9±0.6	28.8±0.5
B1-32	3462 ± 4	1.94 ± 0.2	0.97 ± 0.1	26.7±0.3	21.2±0.3
B1-33	4832 ± 8	2.71 ± 0.4	1.35 ± 0.2	35.9±0.6	29.6±0.5
B1-34	4049 ± 4	2.27 ± 0.2	1.13 ± 0.1	30.3±0.3	24.8±0.2
B1-35	4070 ± 7	2.28 ± 0.4	1.14 ± 0.2	30.4±0.6	25.0±0.5
B2-1	5515 ± 2	3.09 ± 0.2	1.54 ± 0.1	45.9±0.2	33.5±0.2
B2-2	4394 ± 4	2.46 ± 0.2	1.23 ± 0.1	35.0±0.3	26.8±0.2
B2-3	3054 ± 2	1.71 ± 0.1	0.86 ± 0.1	30.5±0.2	18.2±0.1
B2-4	4500 ± 8	2.52 ± 0.5	1.26 ± 0.2	37.6±0.6	27.3±0.5
B3-1	4786 ± 2	2.68 ± 0.1	1.3 ± 0.1	30.8±0.2	29.7±0.1

Table 4.9 Absorbed doses, Effective doses and Health hazards of samples

Sample Name	Absorbed Dose (D) (nGy/h)	Effective dose (ED_{in}) ($mSv \cdot y^{-1}$)	Effective dose (ED_{out}) ($mSv \cdot y^{-1}$)	Internal Health Hazard (H_{in})	External Health Hazard (H_{ex})
B3-2	1753 ± 3	0.98 ± 0.2	0.49 ± 0.1	11.7±0.2	10.8±0.2
B3-3	3483 ± 4	1.95 ± 0.2	0.98 ± 0.1	22.7±0.3	21.5±0.3
B3-4	2676 ± 4	1.5 ± 0.2	0.75 ± 0.1	18.9±0.3	16.5±0.3
B4-1	1537 ± 3	0.86 ± 0.2	0.43 ± 0.1	11.1±0.2	9.4±0.2
B4-2	2597 ± 5	1.45 ± 0.3	0.73 ± 0.2	17.0±0.4	16.0±0.3
B4-3	1855 ± 3	1.04 ± 0.2	0.52 ± 0.1	12.8±0.2	11.4±0.2
B4-4	542 ± 1	0.3 ± 0.05	0.15 ± 0.02	3.9±0.1	3.3±0.1
B5-1	4633 ± 7	2.59 ± 0.4	1.34 ± 0.2	31.5±0.5	28.6±0.4
B5-2	2898 ± 5	1.62 ± 0.3	0.81 ± 0.1	20.5±0.4	17.8±0.3
B5-3	4517 ± 7	2.53 ± 0.4	1.26 ± 0.2	30.3±0.5	27.9±0.4
B5-4	4617 ± 5	2.59 ± 0.3	1.29 ± 0.1	31.1±0.4	28.5±0.3
B6-1	1510 ± 1	0.85 ± 0.1	0.42 ± 0.4	9.7±0.1	9.3±0.1
B6-2	1529 ± 3	0.86 ± 0.2	0.43 ± 0.1	9.7±0.2	9.4±0.2
B6-3	1633 ± 3	0.91 ± 0.2	0.46 ± 0.1	10.5±0.2	10.1±0.2
B6-4	1545 ± 3	0.86 ± 0.2	0.43 ± 0.1	9.9±0.3	9.5±0.2
B6-5	1433 ± 3	0.8 ± 0.2	0.4 ± 0.1	9.1±0.2	8.8±0.2
B7-1	312 ± 1	0.17 ± 0.04	0.09 ± 0.02	2.1±0.05	1.9±0.04
B7-2	294 ± 1	0.16 ± 0.04	0.08 ± 0.02	1.9±0.04	1.8±0.04
B7-3	340 ± 1	0.19 ± 0.01	0.1 ± 0.03	2.3±0.05	2.1±0.05
B7-4	341 ± 1	0.19 ± 0.01	0.1 ± 0.04	2.3±0.05	2.1±0.05

5. CONCLUSION

In this thesis, Eskişehir-Beylikova rare earth elements field were analyzed by gamma spectrometric method for determining U, Ra, Th and K radioactivity of the soil and ore samples. These measured activity values using for probable dose estimation for the mine workers.

After the activity values are determined, these results are reported according to the sample locations marked in site map. For instance, Table 5.1 shows location B1 where is outside the gallery. There is no systematic trend in activity results, but they are always measured higher than surface soil samples. However, B6 and B7 represents soil samples taken from the outside of the ore site, and these samples have low activity values compared to other section as expected.

Table 5.1 B1 location outside activity results

Location (outside)	**Measured Activity ($Bq \cdot kg^{-1}$)**			
(B1-1) – (B1-24)	**^{238}U**	**^{232}Th**	**^{226}Ra**	**^{40}K**
Maximum	4793±54	5643±11	6030±10	170±1
Minimum	1443±40	1197±5	1348±4	40±2
Mean	2430±46	3120±7	2387±7	111±1

Table 5.2 B1 location inside activity results

Location (inside)	**Measured Activity ($Bq \cdot kg^{-1}$)**			
(B1-25) – (B1-35)	**^{238}U**	**^{232}Th**	**^{226}Ra**	**^{40}K**
Maximum	2906±36	6049±15	2502±8	181±2
Minimum	1912±49	3534±9	1720±3	124±1
Mean	2264±39	4731±11	2100±5	150±2

Table 5.3 B2 location outside activity results

Location (outside)	Measured Activity (Bq·kg^{-1})			
(B2-1) – (B2-4)	**^{238}U**	**^{232}Th**	**^{226}Ra**	**^{40}K**
Maximum	4420±17	5463±8	4580±7	184±1
Minimum	3225±30	1543±4	3047±5	44±1
Mean	4068±27	4052±6	3990±6	135±1

Table 5.4 B3 location outside activity results

Location (outside)	Measured Activity (Bq·kg^{-1})			
(B3-1) – (B3-4)	**^{238}U**	**^{232}Th**	**^{226}Ra**	**^{40}K**
Maximum	1046±41	6203±12	903±3	1057±3
Minimum	462±43	2514±7	319±1	213±2
Mean	778±42	3970±9	522±2	534±3

Table 5.5 B4 location outside activity results

Location (outside)	Measured Activity (Bq·kg^{-1})			
(B4-1) – (B4-4)	**^{238}U**	**^{232}Th**	**^{226}Ra**	**^{40}K**
Maximum	681±25	3851±7	616±2	1149±4
Minimum	226±9	647±2	212±1	861±2
Mean	481±18	2345±4	355±1	1079±3

Table 5.6 B5 location outside activity results

Location (outside)	Measured Activity (Bq·kg^{-1})			
(B5-1) – (B5-4)	**^{238}U**	**^{232}Th**	**^{226}Ra**	**^{40}K**
Maximum	1489±37	6704±13	1087±7	291±3
Minimum	1284±59	3925±10	868±4	120±2
Mean	1379±47	5969±11	976±6	200±2

Table 5.7 B6 location soil sample activity results

Location (soil)	**Measured Activity (Bq·kg^{-1})**			
(B6-1) – (B6-5)	**^{238}U**	**^{232}Th**	**^{226}Ra**	**^{40}K**
Maximum	401±39	2443±7	156±1	1057±3
Minimum	276±30	2167±5	98±1	1001±2
Mean	352±36	2297±6	131±1	1057±3

Table 5.8 B7 location soil sample activity results

Location (soil)	**Measured Activity (Bq·kg^{-1})**			
(B7-1) – (B7-4)	**^{238}U**	**^{232}Th**	**^{226}Ra**	**^{40}K**
Maximum	82±16	477±2	65±1	372±1
Minimum	63±23	410±1	52±1	356±1
Mean	73±19	446±2	61±1	366±41

Table 5.9 shows gamma concentration index which is a measure of total gamma dose due to ^{226}Ra, ^{232}Th and ^{40}K. It is worth noting that total gamma issue cannot be neglected during REE mining works. Because they are always greater than unity given for public.

Table 5.9 Gamma concentration indexes of samples

Sample Name	Gamma Concentration Index (I)	Sample Name	Gamma Concentration Index (I)	Sample Name	Gamma Concentration Index (I)
B1-1	23.14 ± 0.4	B1-21	17.4 ± 0.2	B3-2	13.99±0.23
B1-2	30.01 ± 0.45	B1-22	23.6 ± 0.38	B3-3	27.87±0.33
B1-3	18.04 ± 0.18	B1-23	19.71 ± 0.31	B3-4	21.2 ± 0.34
B1-4	2.29 ± 0.14	B1-24	25.69 ± 0.36	B4-1	12.13 ± 0.22
B1-5	27.36 ± 0.3	B1-25	26.15 ± 0.46	B4-2	20.78 ± 0.43
B1-6	26.53 ± 0.37	B1-26	26.97 ± 0.49	B4-3	14.73 ± 0.23
B1-7	16.14 ± 0.27	B1-27	28.2 ± 0.15	B4-4	4.28 ± 0.07
B1-8	22.08 ± 0.36	B1-28	37.48 ± 0.41	B5-1	36.88 ± 0.57
B1-9	26.74 ± 0.26	B1-29	24.84 ± 0.31	B5-2	22.95 ± 0.37
B1-10	24.8 ± 0.13	B1-30	28.28 ± 0.14	B5-3	36.03 ± 0.54
B1-11	21.04 ± 0.23	B1-31	36.93 ± 0.63	B5-4	36.8 ± 0.37
B1-12	28.24 ± 0.4	B1-32	27.08 ± 0.33	B6-1	12.1 ± 0.12
B1-13	30.59 ± 0.26	B1-33	38.01 ± 0.59	B6-2	12.26 ± 0.23
B1-14	27.96 ± 0.33	B1-34	31.82 ± 0.27	B6-3	13.08 ± 0.25
B1-15	16.02 ± 0.18	B1-35	31.98 ± 0.58	B6-4	12.38 ± 0.27
B1-16	21.10 ± 0.37	B2-1	42.63 ± 0.19	B6-5	11.5 ± 0.22
B1-17	30.02 ± 0.32	B2-2	34.2 ± 0.27	B7-1	2.48 ± 0.06
B1-18	35.22 ± 0.25	B2-3	22.84 ± 0.15	B7-2	2.35 ± 0.05
B1-19	17.66 ± 0.21	B2-4	34.76 ± 0.64	B7-3	2.72 ± 0.11
B1-20	25.40 ± 0.37	B3-1	38.37 ± 0.16	B7-4	2.72 ± 0.12

Tables 5.10 to 5.15 show that in Beylikova mining site, health hazard indexes (H_{in} and H_{ex}) as well as gamma concentration index(I) are also found to be higher than unity for public.

Table 5.10 B1 location outside dose and hazard index results

Location (B1-1)(B1-24) (Outside)	Absorbed Dose (D) (nGy/h)	Effective dose (ED_{in}) ($mSv \cdot y^{-1}$)	Effective dose (ED_{out}) ($mSv \cdot y^{-1}$)	Internal Health Hazard (H_{in})	External Health Hazard (H_{ex})
Mean	2993	1.7	0.8	22	18
Standard Deviation	762	0.4	0.2	6	5
% CVO	22	23	28	27	28

Table 5.11 B1 location inside dose and hazard index results

Location (B1-25)(B1-35) (Inside)	Absorbed Dose (D) (nGy/h)	Effective dose (ED_{in}) ($mSv \cdot y^{-1}$)	Effective dose (ED_{out}) ($mSv \cdot y^{-1}$)	Internal Health Hazard (H_{in})	External Health Hazard (H_{ex})
Mean	3914	2.2	1.1	29	24
Standard Deviation	572	0.3	0.1	4	4
% CVO	15	16	15.1	14	15

Table 5.12 B2 location dose and hazard index results

Location (B2-1)(B2-4) (Outside)	Absorbed Dose (D) (nGy/h)	Effective dose (ED_{in}) ($mSv \cdot y^{-1}$)	Effective dose (ED_{out}) ($mSv \cdot y^{-1}$)	Internal Health Hazard (H_{in})	External Health Hazard (H_{ex})
Mean	4365	2.4	1.2	37	26
Standard Deviation	934	0.4	0.2	8	5
% CVO	23	17	17	20	22

Table 5.13 B3 location dose and hazard index results

Location (B3-1)(B3-4) (Outside)	Absorbed Dose (D) (nGy/h)	Effective dose (ED_{in}) ($mSv \cdot y^{-1}$)	Effective dose (ED_{out}) ($mSv \cdot y^{-1}$)	Internal Health Hazard (H_{in})	External Health Hazard (H_{ex})
Mean	3174	1.8	0.9	23	19
Standard Deviation	1212	0.7	0.3	10	7
% CVO	39	38.6	38.7	46	38

Table 5.14 B4 location dose and hazard index results

Location (B4-1)(B4-4) (Outside)	Absorbed Dose (D) (nGy/h)	Effective dose (ED_{in}) ($mSv \cdot y^{-1}$)	Effective dose (ED_{out}) ($mSv \cdot y^{-1}$)	Internal Health Hazard (H_{in})	External Health Hazard (H_{ex})
Mean	1632	0.9	0.5	11	10
Standard Deviation	740	0.4	0.2	5	4
% CVO	44	46	39	42	40

Table 5.15 B5 location dose and hazard index results

Location (B5-1)(B5-4) (Inside)	Absorbed Dose (D) (nGy/h)	Effective dose (ED_{in}) ($mSv \cdot y^{-1}$)	Effective dose (ED_{out}) ($mSv \cdot y^{-1}$)	Internal Health Hazard (H_{in})	External Health Hazard (H_{ex})
Mean	4166	2.3	1.2	28	25
Standard Deviation	786	0.5	0.2	6	5
% CVO	19	20	20	18	20

Table 5.16 B6 location dose and hazard index results

Location (B6-1)(B6-5) (Outside)	Absorbed Dose (D) (nGy/h)	Effective dose (ED_{in}) ($mSv \cdot y^{-1}$)	Effective dose (ED_{out}) ($mSv \cdot y^{-1}$)	Internal Health Hazard (H_{in})	External Health Hazard (H_{ex})
Mean	1530	0.9	0.5	10	9
Standard Deviation	72	0.05	0.02	0.4	0.4
% CVO	5	5	3.8	4	4.2

Table 5.17 B7 location dose and hazard index results

Location (B7-1)(B7-4) (Outside)	Absorbed Dose (D) (nGy/h)	Effective dose (ED_{in}) ($mSv \cdot y^{-1}$)	Effective dose (ED_{out}) ($mSv \cdot y^{-1}$)	Internal Health Hazard (H_{in})	External Health Hazard (H_{ex})
Mean	322	0.2	0.05	2.2	2
Standard Deviation	23	0.01	0.01	0.1	0.1
% CVO	7	6.3	6.5	7.3	7.2

On the other hand, we observe that B7 soil sample have lowest activity value which is expecting because of its surface soil that not expected ore content in soil sample.

In generally we observe that activity of ^{232}Th is above the certain value it means generally ^{232}Th activity is high independent from the location but we can't say the same thing ^{238}U and ^{40}K activity so we can conclude that ^{232}Th is more common ore in this area.

After all these evidence, we can calculate the absorbed dose and effective dose terms. These dose calculation making by assumption that miners work four hours in a day, five days in a week and fifty weeks in a year. Similar studies can be found in the literature which takes into account not only gamma doses but also radon exposure calculation resulting in dose. Unlike other research we don't have radon gas measurement equipment and therefore we compare our gamma dose calculations with them.

In first study it is investigated for rare earth elements field in northwestern of Vietnam. They are employing CR-39 track detector in fifty-one point in three different regions. They calculate maximum effective dose for the first region is 22.0 ± 0.9 ($mSv \cdot y^{-1}$), maximum effective dose for the second region is 15.2 ± 0.7 ($mSv \cdot y^{-1}$) and maximum effective dose for the third region is 4.6 ± 0.5 ($mSv \cdot y^{-1}$) (Khanh Phon L.etc.2015).

In second study, State Uranium Company DIAMO which is located in Dolni Rozinka, region of Czech Republic are planning. Their study in thirteen different departments and they use personal dosimeter ALGADE with TL dosimeter. They report that maximum effective dose 0.3 ($mSv \cdot y^{-1}$) and minimum effective dose is 0.08 ($mSv \cdot y^{-1}$) (Otahall P. et. 2014).

Third study is done in Lambapur and Peddagattu uranium mining area which is located in Andhra Pradesh region of India. In sixteen different regions, they use micro-controller based mR-survey meter (type ER-709: Nucleonix Systems Private Limited, India) in addition to the gamma spectroscopy.

They found that the ^{238}U activity value is maximum 176($Bq \cdot kg^{-1}$) and minimum 100($Bq \cdot kg^{-1}$), ^{232}Th activity value is maximum 116($Bq \cdot kg^{-1}$) and minimum 64($Bq \cdot kg^{-1}$), ^{40}K activity value is maximum 373 ($Bq \cdot kg^{-1}$) and minimum 309 ($Bq \cdot kg^{-1}$).

Based on gamma radioactivity results they estimate maximum total dose rate is 165.5 ($nGyh^{-1}$) and minimum total dose rate is 100.6 ($nGyh^{-1}$). (Reddy V.K etc. 2012)

The other study is done in Brazilian underground mining area. They are planning their studies in six different regions and they use E-PERM Electrets Ion Chamber (Radelec, Inc.) and CR-39 nuclear track detector (Landauer). They calculate maximum effective dose 21 ($mSv \cdot y^{-1}$) and minimum effective dose is 1 ($mSv \cdot y^{-1}$) (Santos Talita O. etc. 2014)

In addition, mineralized zone which is located in Himachal Pradesh region of India is investigated. In twenty-two different regions using gamma spectroscopy method for determining activity values of ^{238}U, ^{232}Th and ^{40}K. They find the ^{238}U activity value is maximum 61.6 ± 1.3($Bq \cdot kg^{-1}$) and minimum 18.4 ± 0.8($Bq \cdot kg^{-1}$), ^{232}Th activity value is maximum 69.6 ± 1.6($Bq \cdot kg^{-1}$) and minimum 39.3 ± 0.6 ($Bq \cdot kg^{-1}$), ^{40}K activity value is maximum 650 ± 2 ($Bq \cdot kg^{-1}$) and minimum 285 ± 0.3 ($Bq \cdot kg^{-1}$).
Based on the radioactivity results, they calculate maximum absorbed dose rate is 89.55 ($nGyh^{-1}$) and minimum total dose rate is 52.8 ($nGyh^{-1}$). They calculate, annual effective dose indoor values maximum 0.44($mSv \cdot y^{-1}$), minimum 0.25 ($mSv \cdot y^{-1}$) and annual effective dose outdoor values maximum 0.10($mSv \cdot y^{-1}$), minimum 0.06 ($mSv \cdot y^{-1}$). They calculate gamma concentration index in the range of 0.31–0.53, with an average value of 0.39 respectively (Singh P. etc. 2016).
In our study, the maximum external gamma dose calculated to be 3.1 $mSv \cdot y^{-1}$in the gallery, and 1.54 $mSv \cdot y^{-1}$for open area, mean gamma dose calculated 1.85 $mSv \cdot y^{-1}$in the gallery and 0.93 $mSv \cdot y^{-1}$for open area. The estimated doses for the mine workers are due to mainly ^{226}Ra and ^{232}Th series nuclides.

In the light of these results, we observed relatively higher activities and external gamma dose values.

After these findings we can easily say that that since effective dose rate cannot exceed the 1 mSv per year for public and also gamma concentration index should be under the 1 value, this mining site is still higher as minimum value of 2.29±0.014, given in Table 5.9.

The activity concentrations measurements performed in this study provide preliminary findings site related relatively high dose risk, thus implying to take radiation protection measures for miners in case of complex ore mining process in Beylikova. The doses calculated in this preliminary study were made considering only the dose values exposed due to gamma radiation. Radon and thoron gas, which make up a large part of the internal exposure of the workers, are present in the soil and the rocks. After determination of radon concentrations in rare earth elements mining area, radon dose concentration should be decreasing under the limit value that 300Bq/m^3 (ICRP, 2018) or Turkish Regulation limits up to 1000Bq/m^3 at workplaces.

It is worth noting that since external health hazard index is estimated to be 21 and internal health hazard index is 27 for inside gallery, this implies that these values also should be reduced for mine workers even if an open gallery mining process is implemented because of possible radon and thoron exposure to the lungs.

In conclusion, especially ^{226}Ra radioactivity values are found higher than expected in the complex ore samples collect from Beylikova mine site, thus resulting in higher doses rather than ^{238}U and ^{232}Th radioactivity values. Some of the collected samples contain more than % 0.1 ^{232}Th and non-negligible amount of ^{238}U. Hence, this thesis study based on Beylikova-Sivrihisar complex ore site give the first results on their radioactivity contents and their possible doses to the mining workers. This study indicated that the calculated gamma dose values always exceed the public dose limit of 1 mSv/y, thus causing higher health hazard indexes. This implies that additional radiation protection measures should be taken during complex ore mining process even if an open gallery mining is implemented in Beylikova ore mining area. In future, this work can be extended to other mine galleries in this area by taking more samples, thus giving the experimental findings about miners' doses that can then be reduced the permissible limits under the licensing of ore mining operation in this area. It is worth noting that total dose issue is still an important point in Beylikova mining process due to mainly ^{226}Ra content because the fraction of radon (^{222}Rn) in the inhaled air might cause to exposure to miners' lungs.

REFERENCES

Ahmed S.N. 2007 **"**Physics and Engineering of Radiation Detection" First edition Queen's University, Kingston, Ontario

Akkaya G. 2011 "Bursa ili toprak numunelerinde radyonüklid dağılımının incelenmesi" Doctoral thesis, Uludağ University Department of Physics, Bursa

Anonymous, 1999 Council Recommendation of 1999 on the limitation of exposure of the general public.

Anonymous, 2017 "Dünyada Ve Türkiye'de Nadir Toprak Elementleri" Maden Teknik Arama Genel Müdürlüğü Fizibilite Etütleri Daire Başkanlığı Mesut ŞAHİNER, Yusuf Ziya AKGÖK, Murat ARSLAN, M.Haluk ERGİN, 2017

Anonymous, 2019-a Laboratoire National Henri Becquerel (http://www.lnhb.fr/nuclear-data/module-lara/) 12.02.2018

Anonymous, 2019-b NIST https://physics.nist.gov/PhysRefData/Xcom/html/xcoml.html 08.11.2017

Anonymous, 2019-c Lara web index http://www.nucleide.org/Laraweb/index.php 15.11.2017

Atik Ş. 2014 Indoor radon measurements in the Abant İzzet Baysal university campus. Master thesis, Abant İzzet Baysal University Department of Physics, Bolu.

Debertin K. 1988 Helmer R. G. Gamma and X-ray spectrometry with semiconductor detectors, North Holland, Amsterdam, 1988.

Genie 2000 Handbook, Canberra Industries, Inc. Printed in the USA

Gillot, P.Y. and Hildenbrand, Anthony and Lefevre, J.C. and Livadie, C. (2006) The K/Ar dating method: principle, analytical techniques, and application to Holocene volcanic eruptions in Southern Italy. 18. 55-66.

Huy, N.Q. and Luyen, T.V. 2004 A method to determine P238PU activity in enviromental soil samples by using 63, 3 keV photopeak-gamma HPGe spectrometer. Applied Radiation and Isotopes, 61(6); 1419-1424.

IAEA, 2019 International Atomic Energy Agency Publications Factsheets 'Radiation in Everyday Life'

ICRP, 1993 Recommendations of the International Commission on Radiological Protection. ICRP Publication 65.

ICRP, 2018 ICRP Recommendations on Radon ICRP ref 4836-9756-8598

Kayabalı İ. 1986, MTA yayınları MTA Genel Müdürlüğü Yayın Serisi no:196 “Türkiye Linyit Envanteri”

Kaplan H. 1977, MTA Enstitüsü Yayın no: 168 “MTA Enstitüsünce bilinen Türkiye yer altı kaynakları envanteri”

Khanh Phon L.2015 Bui Dac Dung, Nguyen Dinh Chau, Tibor Kovacs, Nguyen Van Nam, Duong Van Hao, Nguyen Thai Son, Vu Thi Minh Luan “Estimation of effective dose rates caused by radon and thoron for inhabitants living in rare earth field in northwestern Vietnam”

Khatun M.A. J. Ferdous, M. M. Haque 2018 “Natural Radioactivity Measurement and Assessment of Radiological Hazards in Some Building Materials Used in Bangladesh” Bangladesh 2018

Knoll G. F. 2000 Radiation Detection and Measurement Third Edition. Wiley, 816, New York. 2000.

Krieger, R. 1981 Radioactivity of Construction Materials. Betonwerk Fertigteil-Technique, 47, 468.

Otahal1 P. 2014, I. Burian, M.M. Nasir and Z. Gregor “Radon contribution to the total effective dose of uranium miners”

Reguigui N. 2006 ‘Gamma Ray Spectrometry Practical Information’

Reus, U. and Westmeier, W. 1983 Atomic data and nuclear data tables. Catalog of Gamma-Rays from Radioactive Decay, 29(1-2); 393.

Santos T. O. 2014 Z. Rocha, P. Cruz, V. A. Gouvea, J. B. Siqueira and A. H. Oliveira “Radon dose assessment in underground mines In Brazil”

Singh P. 2016, Prabhjot Singh, Bikramjit Singh Bajwa, Bijay Kumar Sahoo “Radionuclide contents and their correlation with radon-thoron exhalation in soil samples from mineralized zone of Himachal Pradesh, India”

Swedjemark G.A. 1998 'An Overview of Radon Indoors' Radiation Protection 98, Scientific Seminar on Radiation Protection in Relation to Radon.

UNSCEAR, 2000 “United Nations Scientific Committee on the Effects of Atomic Radiation. Source and Effects of Ionizing Radiation. UNSCEAR 2000 Report."

USNRC, 2019 Technical Training Center 'Radiation Terminology' USNRC

Reddy V.K. Gopal Reddy, D. Vidya Sagar, P. Yadagiri Reddy, and K. Rama Reddy 2012, "Environmental radioactivity studies in the proposed Lambapur and Peddagattu uranium mining Areas of Andhra Pradesh, India"

Yücel, H., Çetiner, M.A. and Demirel H. 1998. Use of the 1001 keV peak of P234mPPa daughter of P238PU in measurement of uranium concentration by HPGe gamma-ray spectrometry. Nuclear Instruments and Methods in Physics Section A, 413; 74-82.

Yücel H. 2008. İleri Radyasyon Dedeksiyonu ve Ölçüm Lab. Deneyleri. Ankara Üniversitesi, Nükleer Bilimler Enstitüsü, Ders Notları, Ankara 1-25

Yücel H., Solmaz A.N., Köse E. and Bor D. 2009 **"**Spectral interference corrections for the measurement of ^{238}U in materials rich in thorium by a high resolution gamma-ray spectrometry" Applied radiation and isotopes 67(11), 2049-2056.

Yücel H., Uyar E., Yüksel A.Ö., Güven R 2017 Methodology for determination of correction factors in direct gamma spectrometric measurement of radionuclides in sediments. International Journal of Sediment Research, Vol. 32 (2017), 324-330.

WHO, 2019 World Health Organization Radiation Programme Department of Public Health and Environment Geneva-Switzerland

CURRICULUM VITAE

Name : Süleyman ÖVÜÇ

Birthplace: Van

Birth date: 09.09.1989

Marital status: Married

Foreign language: English

Education:

High school: M.T.S.O. Anadolu Lisesi (2003-2007)

Bachelor degree: Hacettepe University Nuclear Energy Engineering (2008-2015)

Master degree: Ankara University Institute of Nuclear Sciences Department of Medical Physics (2016-2019)